Materials and Structures (2026) 59:194
https://doi.org/10.1617/s11527-026-03091-8

ORIGINAL ARTICLE

A comparative analysis of the thermal conductivity measurement of asphalt concrete under steady-state and transient heat transfer conditions

Duygu Demirtürk · Hande Isik Ozturk · Murat Guler

Received: 12 November 2025 / Revised: 26 February 2026 / Accepted: 4 April 2026
© The Author(s) 2026

Abstract The long-term performance of pavement structures is strongly governed by temperature-dependent distress mechanisms, including rutting and thermally induced stresses. As heat transfer properties regulate internal temperature gradients within asphalt layers, the accurate determination of thermal conductivity is essential for reliable service-life prediction. Yet, accurately assessing the thermal properties of such a complex and heterogeneous material remains challenging due to variations in mixture composition, inconsistent heat transfer mechanisms, and experimental limitations. To overcome these challenges, this work employs both steady-state and transient-state testing methodologies to determine the thermal conductivity of asphalt concrete samples. Following this, the study conducts a detailed comparative evaluation of the two approaches to better understand their strengths and limitations. Accordingly, a new, well-insulated apparatus equipped with a heat flux sensor was designed for the steady-state testing approach, significantly enhancing the thermal insulation process necessary for achieving one-dimensional heat transfer, a capability lacking in current studies. In addition, transient heat transfer experiments were performed using the Hot Disk TPS 2500S instrument. In this study, twelve different mixtures were prepared with two aggregate sources, three distinct air void levels, and two different maximum aggregate sizes, and their thermal conductivities were compared under two heat transfer conditions. The TPS method, which is quick and easy, consistently showed higher values due to aggregate particles in the sensor's contact zone. Conversely, the improved steady-state approach yielded relatively lower but more reliable values, effectively reflecting the sample's thermal conductivity by considering the distribution of mixture components.

Keywords Heat transfer · Thermal conductivity · Asphalt concrete · Transient plane source · Steady-state

1 Introduction

Asphalt concrete, preferred for its high durability, flexibility, ease and speed of construction, cost-effectiveness, smooth surface, water resistance, and adaptability to various conditions, may nevertheless experience thermally induced surface distress due to daily and seasonal temperature variations [1, 2]. When it softens, it becomes more prone to deformation at higher temperatures, whereas at cold temperatures, it becomes brittle, leading to thermal cracks [3–5]. Moreover, asphalt pavements absorb heat due

D. Demirtürk (✉)
Department of Civil Engineering, Ankara Yıldırım Beyazıt University, Ankara, Turkey
e-mail: ddemirturk@aybu.edu.tr

H. I. Ozturk · M. Guler
Department of Civil Engineering, Middle East Technical University, Ankara, Turkey

Published online: 14 April 2026

to their natural dark color [6–8] and substantially affect the land surface temperature (LST) of urban areas [9]. Therefore, a comprehensive understanding of asphalt concrete's thermal properties is necessary to ensure the structural integrity of road infrastructure and its ability to withstand various climatic conditions [10]. Among these properties, thermal conductivity is a fundamental parameter, as it controls heat transfer from the pavement surface to underlying layers and influences the thermal response of the pavement system [11, 12]. It serves as a critical input in applications aimed at mitigating urban heat island effects, enhancing self-healing potential, and enabling thermal energy storage. Furthermore, it plays a crucial role in specialized systems such as asphalt solar collectors designed to improve snow-melting efficiency and solar energy absorption [6, 13–15]. Consequently, accurate determination of thermal conductivity is indispensable for the rational design and performance assessment of these technologies. However, the thermal conductivity measurements in the previous studies are variable and inconsistent due to the measurement methods and heterogeneous structure of asphalt concrete [16–20].

Thermal conductivity of materials is generally determined using either steady-state or transient heat transfer approaches [16, 17]. In the steady-state approach, thermal conductivity is determined when heat flows continuously, reaching a constant heat transfer rate, and the system's temperature remains steady over time [18]. On the other hand, transient heat transfer is measured based on the change in temperature inside a substance over time [19]. Variations in these methods result not only from the different measurement approaches but also from the components of the experimental setups and the types of materials used [20]. Previous research has predominantly employed the guarded hot plate and heat-flow meter techniques to determine the thermal conductivity of asphalt concrete within steady-state regimes [21, 22]. Conversely, more recent investigations have applied transient-based techniques, such as the Transient Hot Wire, Transient Plane Source (TPS), Modified TPS (MTPS), Transient Line Source (TLS), and Modified TLS (MTLS), to assess the thermal conductivity of asphalt concrete under unsteady heat flow conditions [23–26]. Despite these methodological advances, discrepancies between laboratory-based and in-situ thermal conductivity measurements remain common, primarily due to environmental variability, specimen scaling effects, and uncontrolled boundary conditions [27].

Steady-state testing methods are primarily limited by the difficulty of maintaining strictly one-dimensional heat flow and ensuring sufficient thermal insulation under laboratory conditions. Moreover, measurements must continue until the system stabilizes and reaches equilibrium conditions to ensure accurate data collection, which significantly extends the testing time [17, 28]. Tan et al. [29, 30] criticized steady-state methods for their lengthy testing times and unsuitability for building materials. In response to these limitations, Luca and Mrawira [28] developed the UNB k-alpha tester, a device suitable for small sample sizes. Building on this methodology, Carlson et al. [18] introduced a test setup utilizing a cylindrical sample geometry, which enabled the simultaneous assessment of the thermal and mechanical properties of asphalt concrete. Côté et al. [31] also introduced a steady-state method for thermal conductivity cells used with cylindrical asphalt concrete samples to address the limitations related to sample size. Despite these operational limitations, steady-state methods are often regarded as providing relatively reliable results for heterogeneous materials [32]. In contrast, transient techniques offer faster and more practical measurements by analyzing the time-dependent thermal response of the material [16]. Specifically, the TPS method is frequently used to measure the thermal properties of asphalt concrete, where the measurement mainly depends on the thermal resistance of the TPS sensor [33]. However, a significant disadvantage of the TPS method is its limited applicability to heterogeneous materials, such as asphalt concrete, despite providing consistent results for homogeneous materials [34].

Beyond measurement techniques, the thermal conductivity of asphalt concrete is strongly governed by mixture composition, including aggregate type, air void content, and binder characteristics [35, 36]. Asphalt mixtures with higher air void content demonstrate lower thermal conductivity, whereas those containing aggregates with high thermal conductivity exhibit higher values [37, 38]. In particular, the mineralogical composition of aggregates has a significant impact on the thermal conductivity of asphalt mixtures [39]. For instance, aggregates that are rich in minerals like quartz or feldspar have a

higher thermal conductivity compared to aggregates that predominantly contain clay minerals [40, 41]. Accordingly, aggregates are regarded as the key factor influencing the overall heat conduction behavior of asphalt composites [35, 42, 43]. It is known that dense-graded asphalt mixtures usually possess higher thermal conductivity than open-graded mixtures, with larger aggregate sizes further enhancing this characteristic [42]. It is also revealed that the type of bitumen has minimal impact on thermal conductivity due to its smaller proportion in the mix and lower efficiency in conducting heat [31]. In short, selecting optimal mixture properties and implementing correct mix designs can mitigate problems related to thermal behavior [43–45]. Although previous studies have established these fundamental relationships between mixture characteristics and thermal conductivity, they have generally evaluated mixture parameters independent of the experimental method. Consequently, the potential interaction between mixture composition and measurement technique remains insufficiently explored.

This study, for the first time, analyzed and compared the effects of steady-state and transient methods on the thermal conductivity measurements of asphalt concrete. It is essential to note that this comparison was necessary to obtain a reliable thermal conductivity measurement for asphalt concrete. This study not only filled this gap by measuring the thermal conductivity of asphalt concrete samples with varying mixture properties using steady-state and transient test approaches simultaneously but also proposed a novel test setup to overcome the insulation limitations of existing steady-state test setups. Concurrently, the widely used Hot Disk TPS 2500S test device was selected to evaluate the transient heat transfer condition, allowing for a comprehensive comparison of both methods. Ultimately, the aim was to determine whether steady-state or transient methods are more suitable for determining the thermal conductivity of asphalt concrete samples.

2 Materials and mixture properties

2.1 Materials

The asphalt mixes were produced by incorporating basalt and dolomite aggregates together with a 50/70 penetration-grade neat bitumen. The selected aggregate sources are commonly used in road construction in Türkiye. The properties of the aggregates and bitumen were tested according to ASTM standards, and the results are presented in Table 1. The viscosity–temperature relationship of the binder was also determined according to AASHTO T316. Based on these viscosity measurements, the mixing and compaction temperatures of the 50/70 penetration-grade bitumen were established as 155 °C and 145 °C, respectively. In addition to the physical properties presented in Table 1, X-ray powder diffraction (XRD) analysis was conducted to determine the mineralogical composition of the aggregates. As illustrated in Fig. 1, the dolomite aggregate is primarily composed of quartz minerals, whereas the basalt aggregate is predominantly characterized by calcareous phases such as anorthite.

2.2 Mixture properties

In this study, asphalt concrete specimens were designed following the Superpave procedure for mix preparation. The Superpave methodology was selected to better simulate field compaction conditions within a laboratory environment [46]. The aggregate gradations were selected in accordance with the wearing course specifications defined by the Turkish General Directorate of Highways (TGDH/KGM). According to these specifications, wearing course mixtures were classified based on their nominal maximum aggregate size (NMAS), with 19 mm designated as Type 1 and 12.5 mm designated as Type 2. Four mix designs were developed by combining two aggregate sources (basalt and dolomite) with two gradation classes (Type 1 and Type 2). For Type 1, the aggregate gradation limits were similar for both basalt and dolomite, except for filler content, which was 3.4% for basalt and 4% for dolomite to satisfy volumetric requirements. The gradation limits for Type 2 were identical for both basalt and dolomite. The design gradation curves for basalt and dolomite aggregates are presented in Fig. 2a for Type 1 and in Fig. 2b for Type 2, including the corresponding specification limits.

After establishing the design gradations for each mixture type, the bulk specific gravity of the aggregate blend ($G_{sb,blend}$) was determined and listed in Table 2. The computed $G_{sb,blend}$ value was then

Table 1 Properties of aggregates and bitumen used in this study

Bitumen Properties	Standards	Units	Values
Penetration (25 °C)	ASTM D5	0.1 mm	52
Softening Point	ASTM D36	°C	51
Ductility (25 °C)	ASTM D113	cm	> 100
Specific Gravity, G_b	ASTM C70	g/cm^3	1.029
Flash Point	ASTM D92	°C	338
Mixing Temperature (Viscosity = 0.17 Pa.s ± 0.02)	AASHTO T316	°C	155
Compaction Temperature (Viscosity = 0.28 Pa.s ± 0.03)	AASHTO T316	°C	145

Aggregate Properties		Standards	Aggregate types	
			Basalt	Dolomite
Specific Gravity for Coarse Aggregate	Bulk	ASTM C127	2.663	2.781
	SSD		2.723	2.796
	Apparent		2.833	2.824
Water Absorption for Coarse Aggregate (%)			2.260	0.550
Specific Gravity for Fine Aggregate	Bulk	ASTM C128	2.693	2.742
	SSD		2.758	2.764
	Apparent		2.880	2.806
Water Absorption for Fine Aggregate (%)			2.410	0.850
Specific Gravity for Filler		ASTM D854	2.711	2.814
Los Angeles Abrasion (%)		ASTM C131	11.7	18.4

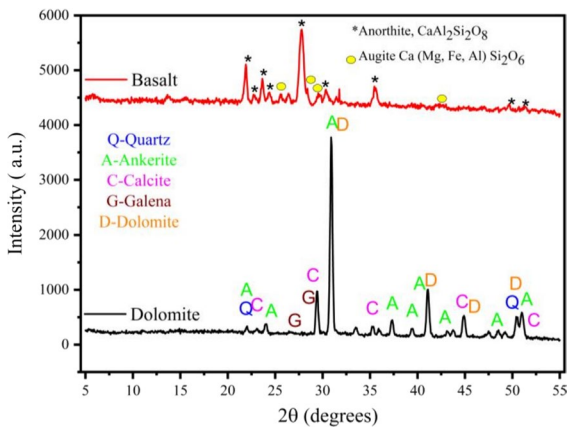
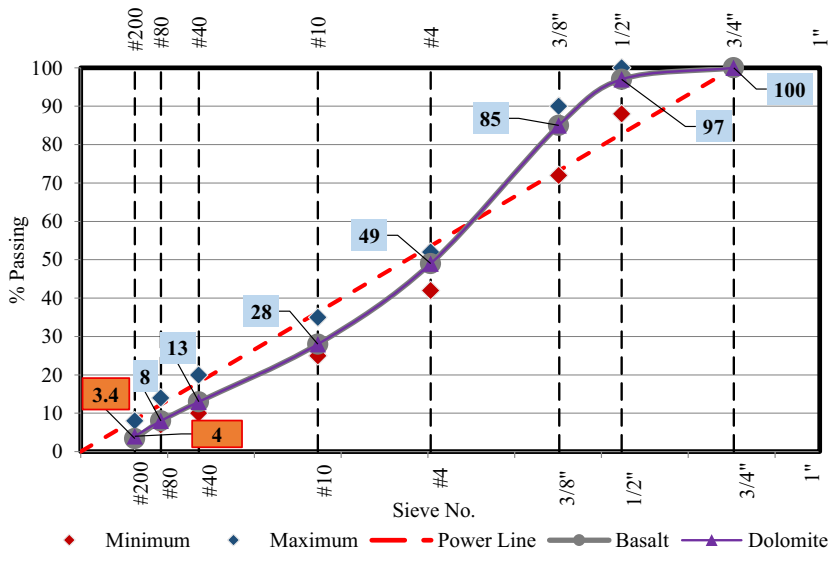


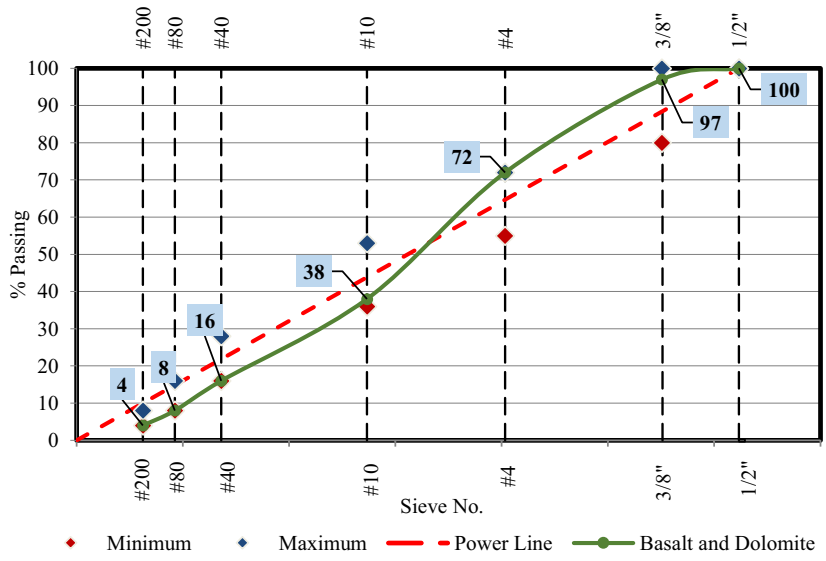
Fig. 1 X-ray diffraction (XRD) intensity versus diffraction angle for basalt and dolomite aggregates

utilized in ascertaining essential volumetric properties, such as VMA, VFA, and air void content (AVC%). For mixtures subjected to a traffic loading range of 3–30 million ESALs, the optimum binder content was determined using 100 gyrations, corresponding to the Superpave N_{design} requirement for this traffic category. This level was considered representative of the intended wearing course application. During the design process, emphasis was given to meeting the volumetric targets specified by TGDH and AASHTO for each mix design. Accordingly, Table 2 shows the optimum binder content and volumetrics of these mixtures.

Each mixture sample was represented by a label that combines the aggregate category, air void content, and gradation classification in sequence. The letters 'B' and 'D' indicated mixtures containing basalt and dolomite aggregates, respectively. Regarding the gradation, the symbols 'T1' and 'T2' corresponded to mixtures with nominal maximum aggregate sizes of 19 mm and 12.5 mm, respectively. Accordingly, the basalt-based mixtures were designated as B4T1 and B4T2, and the dolomite-based mixtures as D4T1 and D4T2, corresponding to Type 1 and Type 2, respectively. In this coding system, "4" represented the target air void content of 4% used in the mix design.



(a)



(b)

Fig. 2 **a** The gradation curves of basalt and dolomite for Type 1 and **b** The gradation curves of basalt and dolomite for Type 2

After the optimum binder content was determined at 4% air void content, further samples were prepared at 2% and 6% air voids with the same binder content. Air void contents of approximately 6% generally represent the initial in situ condition of newly constructed asphalt pavements, whereas values close to 2% represent traffic-induced densification toward the end of service life. Accordingly, these levels were selected to simulate early-life and densified in-service conditions. The target air void contents were achieved by adjusting compaction parameters, specifically the number of gyrations and the density limit, while maintaining constant mixture composition and binder content. Higher gyration levels were applied to obtain approximately 2% air voids, whereas lower gyration levels were used to achieve approximately 6%. This approach ensured that air void content was the only variable among the specimens.

3 Methodology

In this study, two experimental approaches were adopted to evaluate the conductive behavior of

Table 2 Optimum binder content and volumetric properties of four different design mixtures

Mix Design ID	Optimum Binder Content, %*	$G_{sb,blend}$	VMA, %	VFA, %	Bulk Density, kg/m^3	Binder to Filler Ratio
B4T1	5.5	2.678	15.9	74.5	2386	0.665
D4T1	4.9	2.765	14.5	72.2	2487	0.927
Requirements (According to AASHTO and TGDH)	4–7	-	14–16	65–75	–	0.6–1.2
		-	Min. 14	-	-	< 1.5
B4T2	6.2	2.685	15.1	74.3	2430	0.860
D4T2	5.7	2.756	16.1	75	2452	0.805
Requirements (According to AASHTO and TGDH)	4–7	-	14–16	65–75**	–	0.6–1.2
		-	Min. 15	-	-	< 1.5

*The target air void content of 4% used in the mix design

**For design traffic levels > 3 million ESALs, 9.5-mm nominal maximum size mixtures, the specified VFA range shall be 73–76 percent, and for 4.75-mm nominal maximum size mixtures shall be 75–78 percent

asphalt concrete: a custom-developed steady-state heat transfer setup and a transient method using the Hot Disk TPS 2500S instrument. The overall methodology, including specimen preparation, experimental configuration, testing procedure, and data analysis, is briefly outlined in the following sections.

3.1 Laboratory-developed steady-state heat transfer method

All steady-state approaches, including the one developed in this study, are based on Fourier's law, a widely applicable principle stating that thermal conductivity can be determined by the slope of the temperature gradient between parallel surfaces of the sample [47, 48]. This study also improved the practicality of existing steady-state methods and effectively reduced their insulation shortcomings by using a heat flux meter while following relevant standards. ASTM C177 was followed for evaluating heat flow through the sample using a guarded hot-plate arrangement. The overall testing system, incorporating a heat-flux meter, was designed in accordance with ASTM C518. Furthermore, ASTM C1058 was referred to for controlling ambient temperature, and ASTM C1045 procedures were applied to calculate the thermal conductivity of the test samples.

3.1.1 Preparation of test specimens

Based on Fourier's law, the steady-state test method recommends using flat slab specimens with a thickness not exceeding one-third of the maximum linear dimension of the specimen surface through which heat flow occurs (as specified in ASTM C177). In this study, around 1 cm of material was removed from both ends of the Superpave specimens with a diamond saw to achieve a uniform distribution of air voids [49]. Then, as shown in Fig. 3a, the trimmed samples (15 cm in diameter) were cut into two sections, each having a thickness limited to roughly 5 cm. The end surfaces of the slices were cut smoothly to ensure they were aligned with the hot and cold plates without any gaps, thereby facilitating efficient heat transfer. Additionally, a thin layer of thermal silicone paste (See Fig. 3(b)) was applied to the contact surfaces to reduce heat loss during the thermal conductivity measurements, a consideration that had not been previously considered in earlier studies.

3.1.2 Test setup for the steady-state method

The experimental configuration was meticulously designed to enhance the thermal insulation of both the specimen and the heating–cooling plates, thereby minimizing heat loss. As illustrated in Fig. 4, the system consisted of several integrated components, including an insulated test chamber, a refrigeration circulator, a temperature controller, a DC power supply, and a data acquisition unit. The tests were conducted in an insulated chamber containing a hollow cylinder made of interwoven aluminum tubes with outer and inner diameters of 35 cm and 25 cm, respectively. The 35 cm outer cylinder was encased

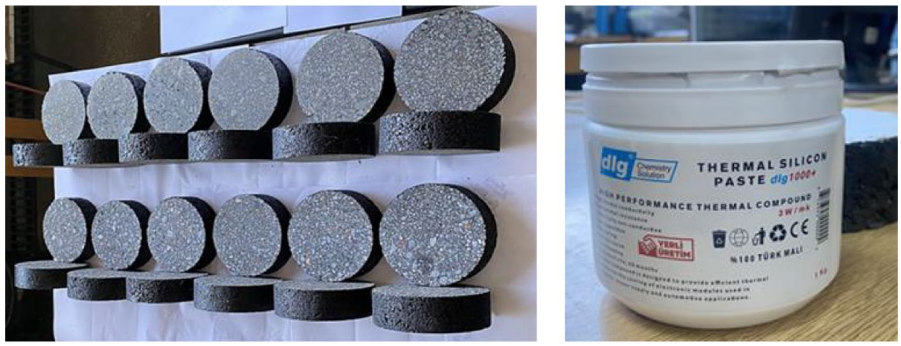


Fig. 3 **a** Sliced samples prepared for the developed steady-state test setup, and **b** thermal silicone compound

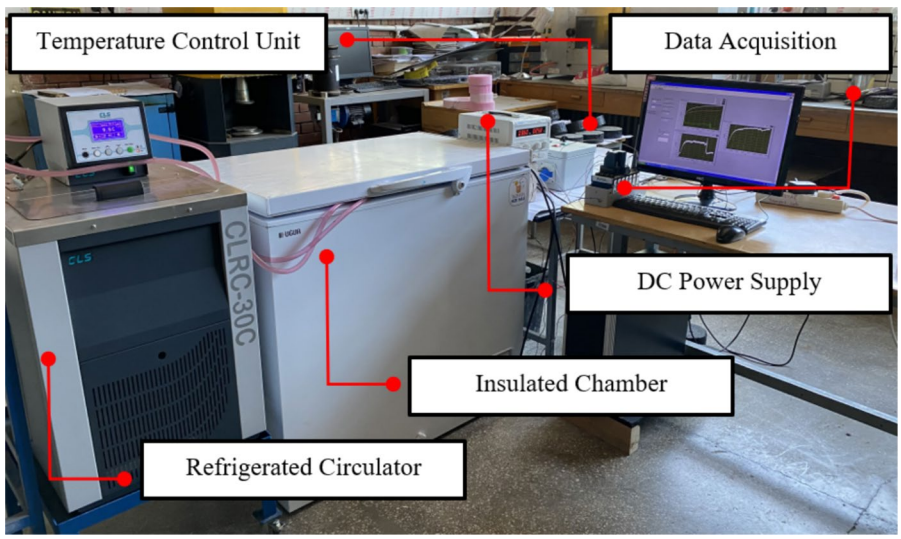


Fig. 4 Overview of the experimental setup

in a 5 cm thick layer of glass wool, a highly efficient insulating material, to reduce heat loss (See Fig. 5). Additionally, the chamber was insulated with 5 cm thick Izocam foam panels, known for their excellent insulation properties. This configuration prevented temperature fluctuations from the surrounding laboratory environment, ensuring a thermally stable condition throughout all measurements of thermal conductivity.

The interior of the insulated chamber was specifically designed to meet the requirements of the current standards, as illustrated in Fig. 5. A heating resistance and an air circulation system were installed to ensure a constant and uniform temperature distribution throughout the chamber. During the testing process, a Resistance Temperature Detector (RTD) sensor was used to monitor the ambient temperature within the chamber. A refrigerated circulator maintained a stable temperature on the cold plate with an accuracy of less than 0.5 °C. In contrast, the hot plate temperature was regulated by varying the electrical current fed to the heating element through a DC power source. Throughout the test, variations in temperature on both plates were continuously tracked with RTD-based temperature probes. Additionally, the temperature controller maintained a uniform ambient condition inside the insulated enclosure and managed the airflow circulation mechanism. Finally, a data acquisition unit continuously logged and observed variations in temperature and heat flux throughout the experiments.

During the tests, the FluxTeq Ultra-09 Plate Heat Flux Sensor (PHFS) was used to measure unidirectional steady-state heat flow across the specimen positioned between the heating and cooling plates (See Fig. 6c), to maintain consistent surface contact

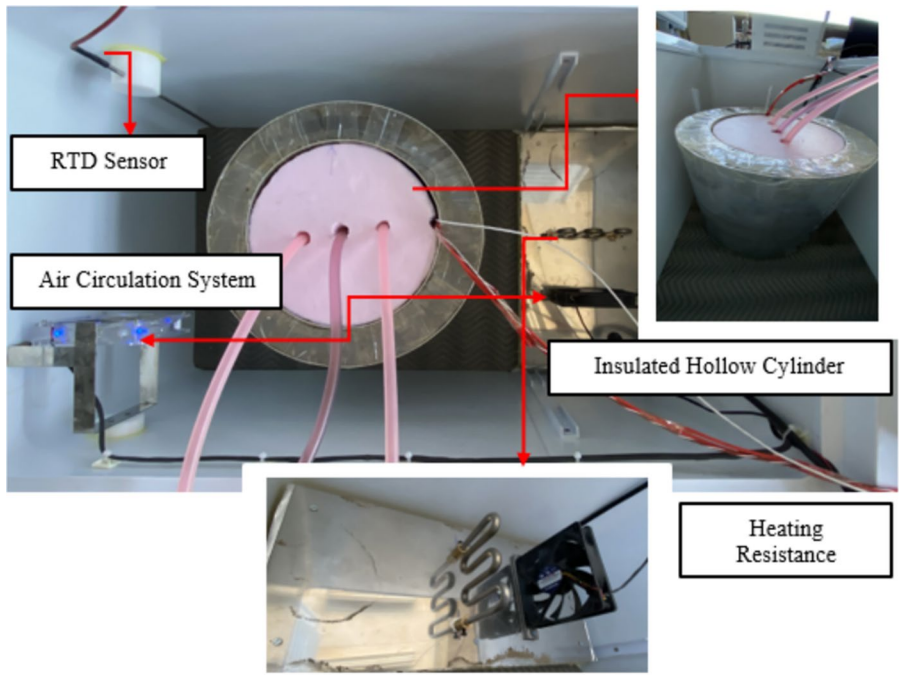


Fig. 5 Interior design of the insulated chamber

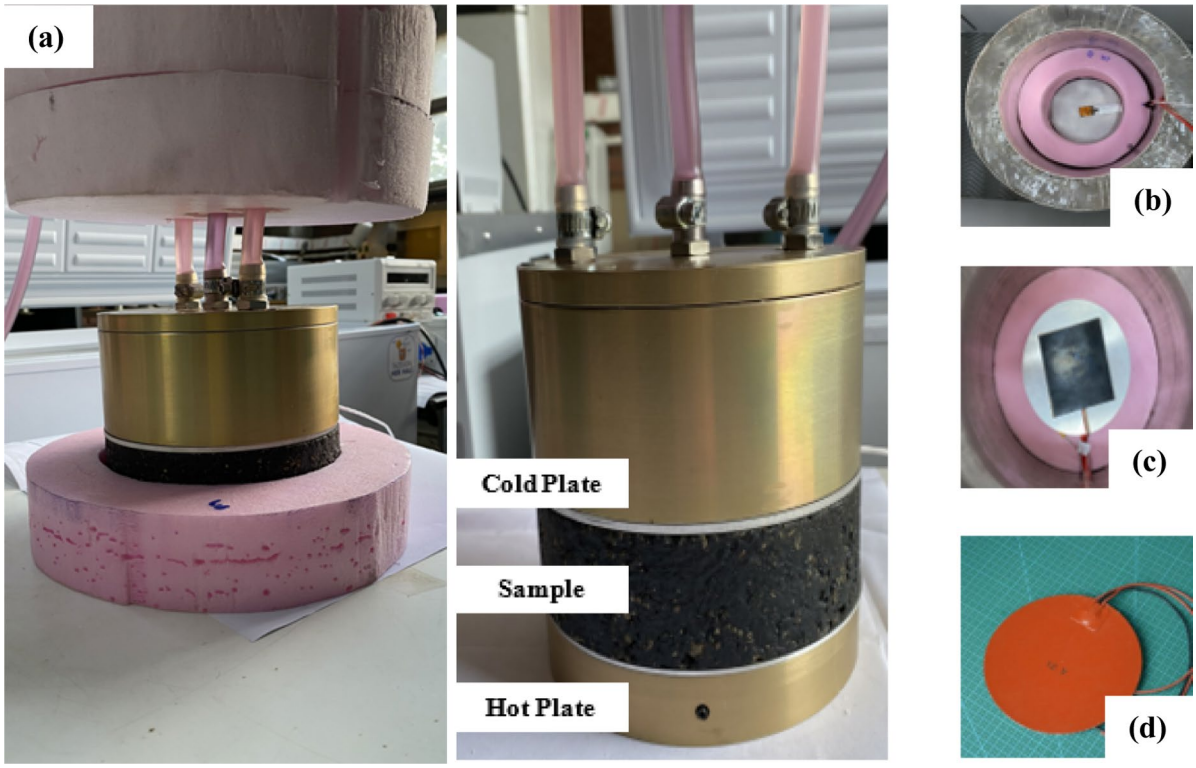


Fig. 6 **a** Arrangement of the internal components within the insulated hollow cylinder, including **b** a temperature probe located beneath the cold plate, **c** a PHFS positioned on the hot plate, and **d** a silicone-based heating element placed below the hot plate

and promote effective heat conduction. Unlike the temperature probe, which measures local interface temperature based on a thermocouple/RTD sensing principle, the PHFS operates according to the thermoelectric effect and directly quantifies one-dimensional heat flux through its calibrated internal thermal resistance layer rather than temperature.

Within this configuration, the setup was configured sequentially, beginning with the heating element at the base (See Fig. 6d), then the hot plate, followed by the PHFS sensor (See Fig. 6c), the test specimen, the cold-side temperature sensor, and finally the cold plate placed on top. Correct positioning of the PHFS within the insulated hollow cylinder was essential to ensure precise measurements and reliable performance. Therefore, it was necessary to mount the sensor firmly on smooth and clean surfaces. In this regard, applying a thin layer of thermal silicone paste between the sensor and the measurement surface, as well as between the temperature sensor and the cold plate, was recommended. Thermal paste was also applied between the hot surface and the bottom of the sensor, as indicated in the PHFS manual, to reduce thermal interface resistance and achieve higher measurement precision. Unlike previous studies, this study primarily focused on reducing the thermal contact resistance in the test setup, with all measures aimed at ensuring a trouble-free measurement of the one-dimensional heat flux of the PHFS.

3.1.3 Measurement procedure

Several preparatory procedures were carried out before initiating the experiments. Initially, the specimens were kept at room temperature for 24 h to stabilize their thermal condition and remove any temperature variations. To maintain a fixed temperature gradient between the heating and cooling plates, the insulated chamber temperature was adjusted to 25 °C, following the recommendations of ASTM C1058. According to ASTM C518, the target temperatures for the hot and cold plates were selected as 40 °C and 10 °C, respectively, corresponding to the ambient laboratory conditions. These temperature settings were essential for applying Fourier's principle effectively and for ensuring the reliable functioning of the PHFS device.

After completing these preliminary steps, the data acquisition unit continuously recorded variations in heat flux and temperature throughout the testing process. The monitoring continued until thermal equilibrium was achieved. When steady-state heat transfer was established between the two plates, the thermal conductivity was determined directly from the PHFS heat-flux readings. For this setup, the system consistently reached equilibrium within approximately 3 h for all samples. Another crucial aspect of the test was maintaining thermal equilibrium in the system to ensure the reliability of the data collected. Therefore, after recording the temperature and heat flux of each specimen for approximately 8 h, the system was left to re-stabilize and reach its initial temperature for another 8 h prior to testing the next specimen. In summary, every specimen was examined under identical experimental conditions.

Finally, the test apparatus was calibrated to maintain measurement accuracy and operational reliability. For the calibration process, the measurements were initially performed using reference materials with established thermal conductivities, such as Izocam foam panels and autoclaved aerated concrete (See Table 3). The calibration factor was calculated as the ratio of the actual thermal conductivity (k_{actual}) to the measured thermal conductivity ($k_{experimental}$) of each material. The "actual" thermal conductivity values were obtained from the manufacturers' product specification sheets. Although the specific testing standards and boundary conditions were not explicitly reported, they were employed solely as reference benchmarks for comparative evaluation. All measurements in the present study were conducted under identical experimental conditions to assess the order of magnitude and to evaluate any potential systematic bias in the proposed measurement setup. Then, the mean value of the obtained calibration factors was determined as 1.07, showing an acceptable deviation of ± 0.15. Consequently, the calibration factor was applied to adjust the readings acquired through the newly designed steady-state testing system.

3.1.4 Details of thermal conductivity calculation

The calculation of thermal conductivity was carried out using measurement results collected from the experimental apparatus as specified in ASTM C1045. While Eq. (1) was used to calculate the thermal resistance, R ($m^2 \cdot °C/W$), Eq. (2) was used to calculate the thermal conductance, C ($W/m^2 \cdot °C$). The following

Table 3 Calibration factor of the experimental setup determined using the thermal conductivity measurements of Izocam foam panel and autoclaved aerated concrete specimens

Izocam Foam Panel		
k_{actual} (W/m·°C)	$k_{experimental}$ (W/m·°C)	Calibration factor
0.035	0.038	0.92
Temperature of Hot Plate: 47.2 °C Temperature of Cold Plate: 10.9 °C Sample Thickness: 50 mm		
Autoclaved Aerated Concrete		
k_{actual} (W/m·°C)	$k_{experimental}$ (W/m·°C)	Calibration factor
0.110	0.090	1.22
Temperature of Hot Plate: 47.2 °C Temperature of Cold Plate: 10.8 °C Sample Thickness: 50 mm		
Calibration Factor of Test Setup: 1.07 ± 0.15		

equations require inputs such as T_h (°C)—the temperature of the hot plate, T_c (°C)—the temperature of the cold plate, Q (W)—the heat flux, A (m^2)—the area perpendicular to the heat flux, and L (m)—the thickness of the sample. Due to the presence of the PHFS and the temperature sensor, these parameters were measured directly in this setup. Therefore, the Fourier's law of heat conduction was applied to determine the thermal conductivity (λ) after the system attained thermal equilibrium, as expressed in Eq. (3). Based on ASTM C1045, Eq. (3) was formulated using the relationships presented in Eqs. (1) and (2).

$$R = \frac{A\left(T_h - T_c\right)}{Q} \tag{1}$$

$$C = \frac{Q}{A\left(T_h - T_c\right)} = \frac{1}{R} \tag{2}$$

$$\lambda = \frac{QL}{A\left(T_h - T_c\right)} \tag{3}$$

3.2 Time-dependent (unsteady-state) heat transfer method

This part discusses the TPS technique as an alternative to the developed steady-state approach. In this approach, the Hot Disk TPS 2500S device illustrated in Fig. 7 was employed. The system consists of a TPS sensor, a holder unit, and the central body of the apparatus, together with clamped specimen sections.

The Hot Disk Thermal Constants Analyzer is capable of evaluating the thermal characteristics of a broad spectrum of materials. It can determine thermal conductivity values ranging approximately from 0.03 W/m·K up to 500 W/m·K for homogeneous, bulk materials. When operated with additional Hot Disk modules, the measurement range can be extended from 0.005 W/m·K to as high as 1800 W/m·K. Moreover, this instrument operates across a broad temperature spectrum, from very low temperatures up to 1000 °C. The Hot Disk TPS 2500S test device uses a transient heat pulse applied through a plane source sensor, which also measures the temperature response. The thermal conductivity and diffusivity of the material under test can be calculated by analyzing the thermal response over time.

3.2.1 Preparation of test specimens

In the TPS technique, accurate determination of thermal conductivity depends on ensuring that the specimen thickness is not less than the radius of the sensor. Previous research has thoroughly established the influence of sensor geometry on the precision of thermal measurements. In this study, a Kapton-insulated sensor (ID 5501, 12.8 mm in diameter), the largest sensor compatible with the TPS configuration, was utilized for testing all asphalt samples [33]. Then, sample preparation started by coring the Superpave

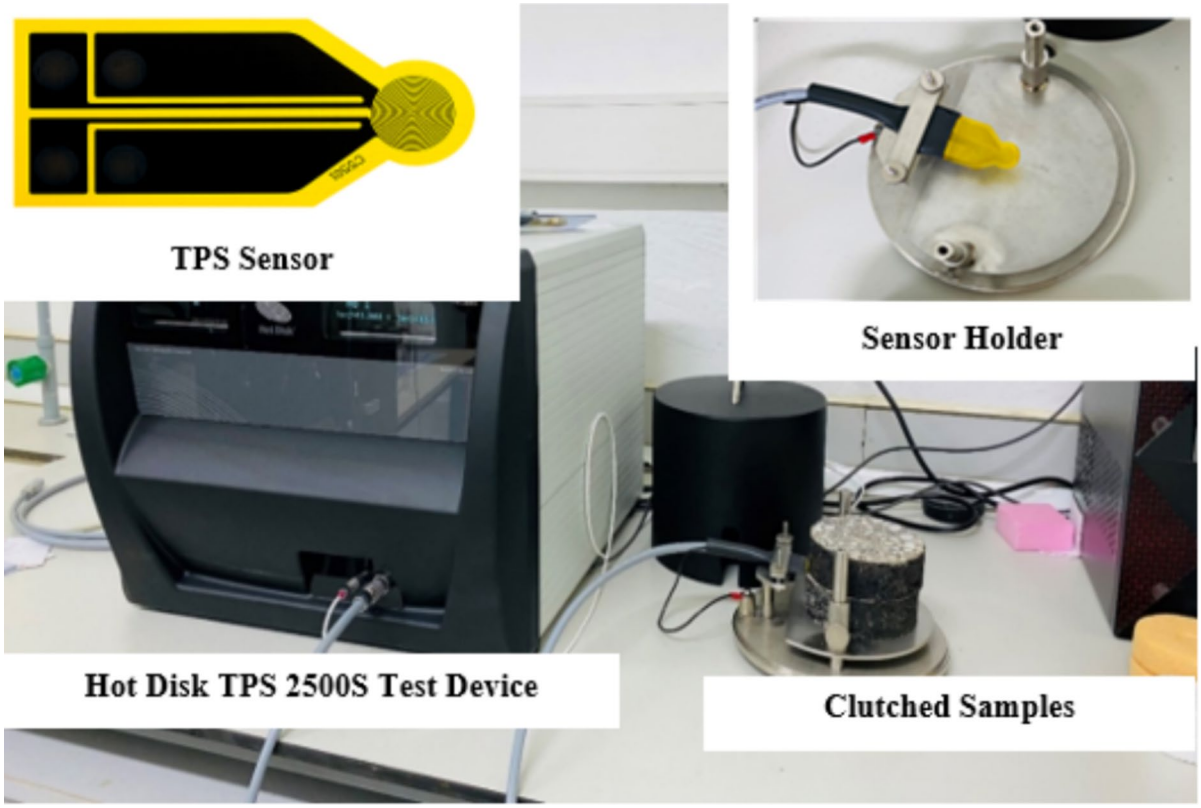


Fig. 7 Hot Disk TPS 2500S testing apparatus and its components

samples to a diameter of 100 mm to fit the TPS sensor holder. Each sample was sectioned into three layers (upper, center, and bottom), maintaining a thickness of 25 ± 0.1 mm, as shown in Fig. 8a. The sensor was positioned between two identical specimen layers—first between the bottom and center sections, and then between the center and top sections. Figure 8 illustrates the sensor placement from different viewing angles. This is because this method allowed the TPS sensor to perform measurements between two identical specimen layers. Additionally, equipment manufacturers suggest considering the effective

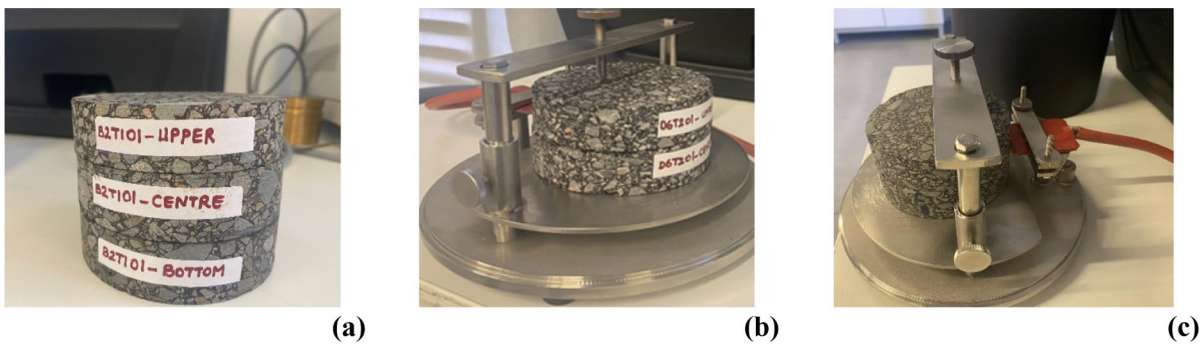


Fig. 8 **a** Transversely sectioned cylindrical specimens, **b** placement of the specimen in the measurement holder and **c** positioning of the TPS sensor between two identical specimen layers

sensing depth or the probing depth when selecting an appropriate sensor–sample configuration. The probing depth is the maximum depth at which the sensor can accurately measure the thermal conductivity. Therefore, when preparing the sample, care should be taken to ensure that the sample thickness is greater than the probing depth.

3.2.2 Measurement procedure

The selection of an appropriate TPS sensor constituted the first phase of the testing process, as mentioned earlier. Since asphalt concrete is a multiphase material, the sensor size is critical as the sensor area may not be in contact with the entire aggregate and mastic if not properly selected. Therefore, to eliminate the sensor size effect in this study, the surface of the sliced samples was divided into four hypotactic zones, as given in Fig. 9. In other words, it is aimed to capture potential variations in thermal conductivity arising from heterogeneous aggregate–mastic distributions and to enhance measurement sensitivity.

Thermal conductivity measurements were repeated at least three times in each zone. A cooling interval of at least 20 min was maintained between successive measurements to allow the samples to reach thermal equilibrium. This procedure was consistently applied to every specimen, and any variation in measurement results was evaluated in the subsequent section to confirm the reliability of this approach. In addition, the heating power and measurement duration were carefully optimized to achieve stable readings. Specifically, these parameters were adjusted to 40 s and 200 mW for basalt samples, and 20 s and 250 mW for dolomite samples, based on the observed residual curve behavior. In summary, the accuracy of the TPS method is largely influenced by the appropriate selection of sensor type, test duration, and input power.



Fig. 9 Schematic illustration of the four symmetrically distributed measurement zones defined on the specimen cross-section

3.2.3 Determination of thermal conductivity using the hot disk constant analyzer

The TPS sensor functions both as a planar heat emitter and as a temperature detector. In operation, it delivers thermal energy to the specimen while simultaneously recording the resulting temperature increase through changes in its electrical resistance. Consequently, the temperature variation within the material is evaluated using Fourier's heat conduction principle, as expressed in Eq. (4).

$$\Delta T(\tau) = \frac{Q}{\pi^{1.5} rk} D(\tau) \tag{4}$$

where Q (W) represents the power supplied by the sensor, k (W/m·°C) denotes the thermal conductivity of the specimen, r (m) is the radius of the sensor, and D is a dimensionless time-dependent function of τ, defined below. In Eq. (5), α (m^2/s) refers to the thermal diffusivity of the material, and t (s) indicates the duration of measurement. The parameter τ is expressed as:

$$\tau = \frac{\sqrt{\alpha t}}{r} \tag{5}$$

As a result, the Hot Disk Constant Analyzer software utilizes these relationships to determine the thermal conductivity of the tested material.

4 Results and discussions

This part of the study presents a comprehensive evaluation addressing three key aspects. First, it contrasts the thermal conductivity values determined by using steady-state and transient testing techniques. Then, it addresses how differences in measurement techniques can shape the observed effect of mixture properties on thermal conductivity. Finally, it reviews the advantages and disadvantages of each test method,

including their strengths, limitations, and appropriateness for asphalt concrete.

4.1 Comparison of thermal conductivity results based on testing method

Thermal conductivity analyses were carried out on duplicate samples taken from each mixture using the designed steady-state test setup. Each duplicate was sectioned into two layers in accordance with the procedure described earlier. To identify these layers, numerical suffixes "01" and "02" were appended to the sample codes (e.g., B2T1-01, B2T1-02). The mean thermal conductivity values of the sliced specimens are reported in Fig. 10.

As illustrated in Fig. 10, the thermal conductivity values of the basalt specimens vary between 0.400 and 0.500 W/m·°C, whereas those of the dolomite specimens are comparatively higher, ranging from 0.550 to 0.800 W/m·°C. The error bars in Fig. 10 show that even though there are fluctuations in the measurements for all samples, they remain negligible.

In the TPS method, two results were obtained for each sample as the sensor took measurements between two sliced samples, as shown in Fig. 8. To determine the thermal conductivity of each layer, the TPS sensor was placed between the center and bottom slices for the bottom measurement, and between the upper and center slices for the top measurement. Based on the operating principle of the TPS sensor, multiple measurements were taken to determine the thermal conductivity of the samples' upper and bottom parts. The average thermal conductivities of the upper and bottom parts of basalt and dolomite samples are presented in Fig. 11, respectively. Similarly, the error bars in Fig. 11 were derived from the

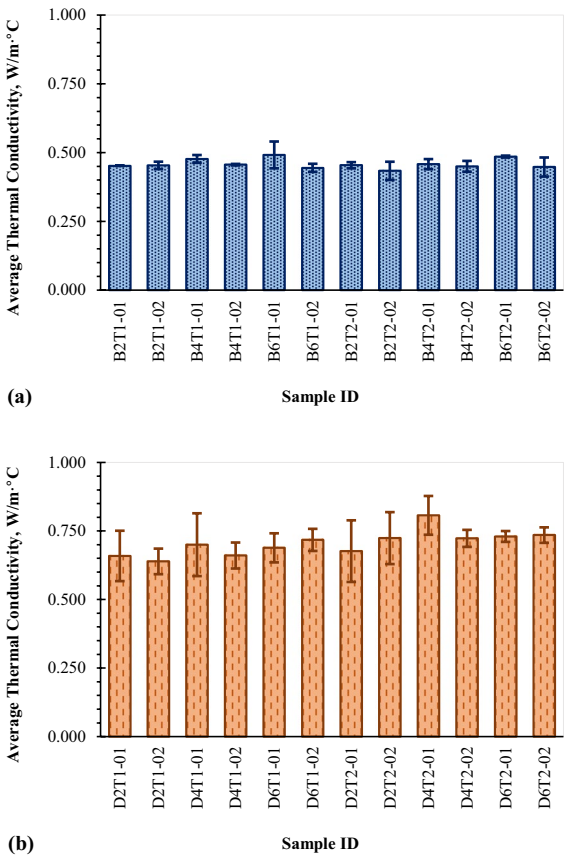


Fig. 10 Comparison of mean thermal conductivity results for basalt **a** and dolomite samples **b** obtained from the developed steady-state setup

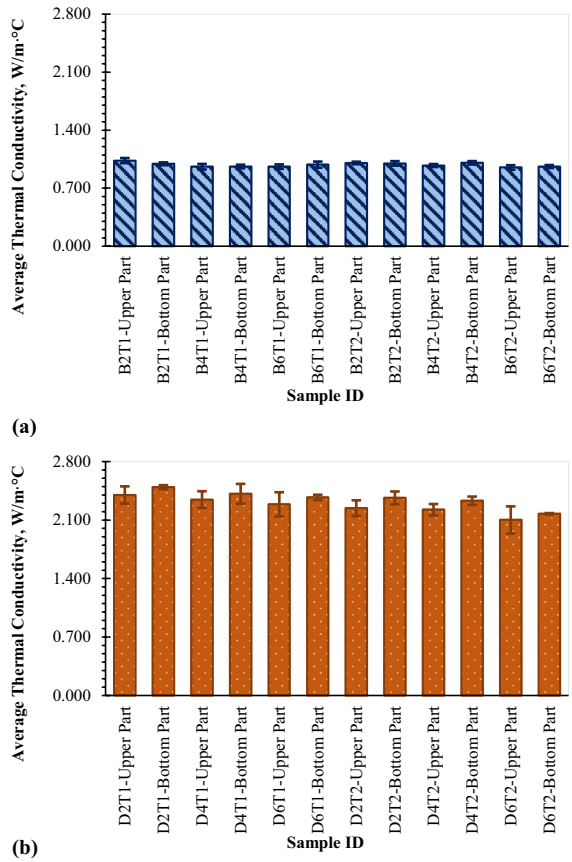


Fig. 11 Comparison of mean thermal conductivity results for basalt **a** and dolomitespecimens **b** measured with the Hot Disk TPS 2500S setup

standard deviations. Similar to the results obtained from the steady-state approach, the dolomite specimens exhibited greater thermal conductivity compared to the basalt specimens.

In summary, Figs. 10 and 11 show that the thermal conductivities measured by the TPS method were higher than those obtained using the developed steady-state method. This phenomenon can be attributed to the fact that when the TPS test was conducted within a shallow contact region containing a large amount of aggregate, the measured thermal conductivity tended to reflect that of the aggregate itself, which inherently possesses a higher thermal conductivity. To confirm this observation using the TPS technique, the thermal conductivity values of the basalt and dolomite aggregates were determined to be 1.41 ± 0.2 W/m·°C and 3.98 ± 0.2 W/m·°C, respectively [50]. These results demonstrated that the aggregates have relatively higher thermal conductivities than other components (0.17 W/m·°C for bitumen, 0.024 W/m·°C for air), which affects the overall ability of asphalt concrete to conduct heat [31].

On the other hand, in the newly developed steady-state setup, heat propagation occurred through the entire thickness of the specimen. Due to the non-uniform distribution of aggregates, fluctuations in heat transfer were observed within the mixture, resulting in a reduced heat-flow intensity through the specimen depth. Additionally, heat transfer was measured using a PHFS, accounting for all the components forming the mixture in a compact form. Consequently, the proposed steady-state approach yielded comparatively lower thermal conductivity values; however, it was considered more representative of bulk specimen behavior, as it captured the composite thermal response of the entire specimen.

4.2 Method-dependent effects of mixture properties on thermal conductivity determination

This section examines the influence of mixture characteristics on thermal conductivity by comparing the mean conductivity values obtained from slices tested with the developed steady-state method to those measured for the upper and bottom sections using the TPS technique. For the steady-state configuration, the statistical analysis was based on 48 independent measurements. Each Superpave specimen was sectioned into two slices and both sections were tested separately, yielding 24 slice measurements for basalt mixtures and 24 for dolomite mixtures. On the other hand, for the Hot Disk TPS measurements, thermal conductivity was determined from four distinct regions on each specimen surface, with a minimum of three repeated measurements per region. In total, 177 individual readings were included in the statistical analysis.

Table 4 shows the mean thermal conductivity results from both test methods and the changes in mixture properties. Samples with identical volumetric properties, made with the same aggregate type and gradation, exhibited different thermal conductivities due to variations in the testing methods. The TPS method, as illustrated in the table, indicates that changes in mixture properties lead to variations in thermal conductivity. However, the findings derived from the newly designed steady-state testing approach did not clearly capture or represent these variations. To clarify this discrepancy, an analysis of variance (ANOVA) was conducted to assess the impact of the mixture properties on thermal conductivity across different testing methods. Accordingly, Table 5 presents the significance levels for the aggregate type, air void content, and maximum aggregate sizes concerning

Table 4 Assessment of thermal conductivity measurements acquired via the developed steady-state configuration and the Hot Disk TPS 2500S method

Tests	Results from the Custom Steady-State Testing Apparatus	Results Obtained Using the Hot Disk TPS 2500S System
Sample ID	Total Sample-Average Thermal Conductivity, W/m·°C	Total Sample-Average Thermal Conductivity, W/m·°C
B2T1	0.419	1.013
B4T1	0.440	0.960
B6T1	0.426	0.972
B2T2	0.429	1.002
B4T2	0.437	0.989
B6T2	0.448	0.955
D2T1	0.561	2.447
D4T1	0.614	2.380
D6T1	0.626	2.330
D2T2	0.586	2.303
D4T2	0.681	2.277
D6T2	0.681	2.138

Table 5 Results of the ANOVA test demonstrating the impact of mixture variables on thermal conductivities determined by the two experimental techniques

Part	Source	Sum of squares	Degrees of freedom	Mean square	F-ratio	*P*-value	Partial eta squared
Developed Steady-State Test Setup							
For all measurements	Air Void Content (%)	0.009	2	0.004	2.136	0.130	0.090
	Maximum Aggregate Size	0.006	1	0.006	2.897	0.096	0.063
	Aggregate Type	0.636	1	0.636	314.903	0.000	0.880
	Total	14.927	48				
	Adjusted $R^2 = 0.871$						
Hot Disk TPS 2500S Test Device							
For all measurements	Air Void Content (%)	0.174	2	0.087	14.806	0.000	0.147
	Maximum Aggregate Size	0.133	1	0.133	22.549	0.000	0.116
	Aggregate Type	71.013	1	71.013	12071.378	0.000	0.986
	Total	459.783	177				
	Adjusted $R^2 = 0.986$						

the thermal conductivities of the samples. Due to the variations in sample preparation and testing procedures for each method, the ANOVA was performed separately on the thermal conductivity results from both the developed steady-state test and the TPS methods.

Accordingly, the ANOVA analysis shows that aggregates are the most significant factor in the thermal conductivity results for both test methods. Nevertheless, within the developed steady-state approach, variations in air-void ratio and maximum aggregate size showed minimal impact on the measured conductivity values ($p > 0.05$). This outcome is primarily related to the volumetric distribution of mixture components throughout the specimen. The non-uniform arrangement of materials at different depths led to slight fluctuations in heat transfer. Owing to the operational characteristics of the PHFS system, such fluctuations in heat-flux readings were inevitable when the internal composition of the sample was inconsistent. Consequently, the influence of air-void content and maximum aggregate size on the overall thermal conductivity became less pronounced.

In the TPS technique, changes in the mixture composition directly influence the microstructural behavior of the material in the sensor–specimen interface region, which significantly affects the measured thermal conductivity, as supported by the ANOVA findings. The geometry, gradation, and surface characteristics of the aggregate particles that come into contact with the sensor govern the heat transfer behavior of the asphalt concrete. Accordingly, the results of TPS method indicated that thermal conductivity gradually declined as the air-void content increased. As presented in Table 4, higher air-void ratios corresponded to slightly lower conductivity values, although the overall differences remained relatively small. As previously mentioned, this study simulated air voids of 2%, 4%, and 6% throughout the pavement's lifetime. Therefore, the results were similar because only a small portion of the 2%, 4%, and 6% air void contents set during design was present on the measurement surface due to the core and cutting process during sample preparation. However, earlier studies indicated that this negative effect was more apparent in samples with higher air void content. Mirzanamadi et al. [33] found that increasing air void content from 2 to 10% significantly reduced the thermal conductivity and diffusion of asphalt concrete by up to 30% in the TPS method. At this point, it is essential to determine how much air void content is represented on the measurement surface to more accurately assess its negative impact on TPS measurement results.

Finally, it is known that the maximum aggregate size directly affects the optimum bitumen content, air void content, degree of compaction, and density of asphalt mixtures. In this study, the contact zone was inevitably affected, which in turn impacted the thermal conductivity measurements in the TPS method. According to Table 4, the results showed that a

coarser gradation led to higher thermal conductivity. This can be attributed to the fact that mixtures with finer gradation (MAS: 12.5 mm) exhibited higher optimum bitumen contents (See Table 2) compared to those with coarser gradation (MAS: 19 mm). Accordingly, as the optimum binder amount increased, the bitumen film separating aggregate particles was expected to alter the heat distribution due to the different thermal responses of the binder and aggregate phases in contact with the TPS probe. Consequently, when the share of coarse aggregates rose, the sensor primarily interacted with particles having greater intrinsic thermal conductivity, leading to higher measured conductivity values for the asphalt mixture.

4.3 Comparative assessment of the newly developed steady-state system and the TPS method

This section presents a comparison between the developed steady-state approach and the TPS technique, focusing on their effectiveness in determining thermal conductivity. The primary distinction between the two methods lies in the duration of testing. Whereas the steady-state measurements required approximately three hours to complete, the TPS tests were accomplished within 5–10 s using the Hot Disk TPS 2500S system. Another notable difference concerned the sample dimensions. The steady-state method employed relatively larger specimens consistent with the guidelines of ASTM C177, while the TPS method utilized smaller ones because of limitations associated with the sensor size and its holder. Moreover, the TPS probe had a smaller diameter than the PHFS sensor adopted in the steady-state setup, which consequently led to variations in the contact area between the sensor and specimen during heat transfer.

The pathways of heat transfer between samples varied according to the testing approach applied in this research. In the custom-designed steady-state system, heat flow was tracked across the entire thickness of the specimen, whereas in the TPS technique, the temperature response was recorded only within the limited probing depth of the sensor. In the TPS method, measurements were restricted by the contact zone at the specimen surface and the sensor's effective depth. Consequently, the steady-state system yielded more comprehensive results since it accounted for heat transfer through the whole sample volume. Overall, the proposed steady-state approach enhanced the precision of thermal conductivity evaluation in heterogeneous materials such as asphalt concrete, leading to more representative results for the entire specimen.

In the developed steady-state test setup, measuring the thermal conductivity of asphalt concrete samples was challenging. Several key parameters were necessary to ensure accurate measurements. Among these, controlling the test temperature was the most critical factor. Variations in the temperature of the apparatus, specimen, or surrounding environment could lead to notable deviations in the measured results, as they directly influenced the response sensitivity of the PHFS system. In addition to temperature stability, factors such as thermal insulation quality, heat loss control, and consistency of the electrical current and voltage supplied to the heating and cooling plates were essential for ensuring proper operation and stability of the system. Unlike earlier studies, this work carefully optimized the insulation process, effectively minimizing unwanted heat losses and environmental fluctuations during testing.

On the other hand, the Hot Disk TPS 2500S monitored temperature response over a brief time interval, usually a few seconds, to determine thermal conductivity. A short time frame lessened inaccuracies that might result from variations in the surrounding temperature. The TPS sensor's focus on the temporary temperature differential guaranteed accurate thermal conductivity measurements, even in external temperature fluctuations. Therefore, it can be inferred that the newly developed steady-state testing system is considerably more sophisticated than the Hot Disk TPS 2500S instrument, primarily because it requires a larger set of equipment and more intricate testing procedures. In summary, Table 6 outlines the key distinctions between the two experimental methods.

5 Conclusion

This study performed a comparative evaluation of the thermal conductivity results determined from the developed steady-state method and the TPS method, under controlled variations in mixture properties. The sensitivity of each measurement method to variations in air void content, nominal maximum aggregate size, and aggregate type were

Table 6 Comparative analysis of developed steady-state and TPS test methods used in this study for measuring the thermal conductivity of asphalt concrete

Parameters	Steady-State Method Developed Steady-State Test Setup	Transient Method Hot Disk TPS 2500S Test Device
Sensor Type	Plate-type heat flux sensor (PHFS, FluxTeq Ultra-09)—dimensions: 9.2 cm × 8.7 cm	TPS sensor model 5501, diameter ≈ 12.8 mm
Test Duration	approx. 3 h	approx. 5–10 s
Sample size	Diameter ≈ 15 cm, thickness ≈ 5 cm; two sliced samples	Diameter ≈ 10 cm, thickness ≈ 2.5 cm; three cored and sliced samples
Heat Transfer Path	Across the full specimen thickness	Within the sensor's probing depth
Effect of Aggregate Type	✓	✓
Effect of Air Void Content	Negligible	✓
Effect of Maximum Aggregate Size	Negligible	✓
Effect Caused by the Initial Temperature of Specimens	✓	✓
Effect Caused by Ambient Thermal Conditions	✓	✓
Level of System Complexity	High	Low

analyzed in addition to the methodological comparison. From this comprehensive evaluation, the following key conclusions have been reached:

- The main difference between the test methods was their working principles: the TPS sensor measured thermal conductivity based on the mix constituents in its contact zone and probing depth, while the PHFS measured it based on the change in heat flux from constituents distributed throughout the entire sample depth.
- The proposed steady-state approach, which accounted for all mixture components throughout the entire specimen thickness, yielded lower thermal conductivity values. Conversely, the TPS technique produced comparatively higher readings, mainly due to the stronger influence of aggregate particles with inherently higher conductivity located within the sensor's contact zone.
- Dolomite-based mixtures consistently exhibited higher thermal conductivity than basalt-based mixtures, regardless of measurement method ($p < 0.001$ for both methods). The very large effect sizes ($\eta^2 p = 0.880$ for the steady-state method and $\eta^2 p = 0.986$ for the TPS method) indicated that aggregate mineral composition was the dominant and method-independent factor governing the heat-transfer behavior of asphalt mixtures.
- Air void content exhibited method-dependent behavior. While AVC was statistically significant in the TPS measurements ($p < 0.001$), but not in the steady-state method ($p > 0.05$). This difference can be attributed to the measurement principles: the steady-state setup captures the bulk thermal response across the entire specimen thickness, averaging volumetric heterogeneities, whereas the TPS method, due to its localized sensing radius near the surface, is more sensitive to variations in air void distribution within the contact zone.
- Similar to the influence of air voids, the nominal maximum aggregate size was found to be dependent on the method. NMAS was statistically significant in the TPS method ($p < 0.001$), but not in the steady-state measurements ($p > 0.05$). This outcome can also be attributed to the operating principle of the PHFS, which tends to produce slight fluctuations in heat flux measurements when the internal distribution of mixture components is non-uniform. In contrast, the TPS method showed that asphalt mixtures with larger maximum aggregate sizes generally exhibited higher thermal conductivity. This is because larger aggregate sizes create more continuous pathways for heat transfer in the TPS method.
- The specimen size requirements varied considerably between the two methods. The proposed steady-state technique was more appropriate for

larger samples, whereas the TPS method required smaller specimens due to restrictions associated with the sensor dimensions and the limited contact zone during measurement.
- Maintaining the reliable performance of the experimental system, along with precise control of heat flux, temperature, and specimen thickness measurements, was an essential requirement to ensure the accuracy and consistency of the thermal property data, particularly under steady-state testing conditions.
- In the TPS method, the characteristics of the mixture significantly affect thermal conductivity measurements by changing the microstructural features of the measurement surface. Factors such as applied heating power, duration of testing, and sensor dimensions also affect the outcomes, thereby influencing the precision and dependability of the measurement process.
- The proposed steady-state testing approach required extensive insulation preparation and multiple procedures to reach steady-state conditions and produce reliable results. Conversely, the TPS technique proved to be more time-efficient and simpler to operate.
- The microstructural configuration of the contact zone is a decisive factor in the accurate interpretation of TPS measurement results, as the probe interacts directly with the mixture's constituent phases, thereby governing the effective thermal conductivity observed during testing. However, this method only evaluates the contact zone and the probing depth of the sensor, leaving concerns about its applicability to asphalt concrete. In contrast, the developed steady-state technique provides a more precise estimation of thermal conductivity by accounting for variations in mix characteristics throughout the sample's depth. Therefore, the steady-state approach is recommended for obtaining accurate thermal conductivity measurements in heterogeneous materials like asphalt concrete.

Consequently, this study clarified the key differences between steady-state and transient (TPS) thermal conductivity measurements in asphalt mixtures, considering the heterogeneous nature. By distinguishing between volumetric and localized sensing approaches, the findings provided a clearer understanding of how each method characterizes the composite thermal behavior of asphalt mixtures. Improving the consistency and representativeness of thermal conductivity measurements enhances the accuracy of temperature predictions and, consequently, can lead to more reliable thermo-mechanical modeling and long-term pavement performance assessments. Thus, future work should include field validation and further integration of laboratory measurements into pavement performance modeling frameworks.

Acknowledgements This research was funded by the Middle East Technical University Scientific Research Projects (METU-BAP) through the research project GAP-303-2021-10743. We appreciate METU-BAP for its financial support.

Author contributions Corresponding Author: Investigation, Conceptualization, Methodology, Writing—Original Draft Preparation. Co-author_1: Supervision, Validation, Writing—Reviewing and Editing. Co_author_2: Supervision, Project Administration, Resources, Writing—Reviewing and Editing.

Funding Open access funding provided by the Scientific and Technological Research Council of Türkiye (TÜBİTAK).

Declarations

Conflict of interest No potential conflict of interest was reported by the author(s).

Open Access This article is licensed under a Creative Commons Attribution 4.0 International License, which permits use, sharing, adaptation, distribution and reproduction in any medium or format, as long as you give appropriate credit to the original author(s) and the source, provide a link to the Creative Commons licence, and indicate if changes were made. The images or other third party material in this article are included in the article's Creative Commons licence, unless indicated otherwise in a credit line to the material. If material is not included in the article's Creative Commons licence and your intended use is not permitted by statutory regulation or exceeds the permitted use, you will need to obtain permission directly from the copyright holder. To view a copy of this licence, visit http://creativecommons.org/licenses/by/4.0/.

References

1. Li Q, Yang G, Si C, Li B (2023) New developments in asphalt pavement: enhancing durability, sustainability, and cost-effectiveness. Coatings 14(1):34. https://doi.org/10.3390/coatings14010034
2. Zhang L, Hoff I, Zhang X, Yang C (2022) Investigation of the self-healing and rejuvenating properties of aged

asphalt mixture containing multi-cavity Ca-alginate capsules. Constr Build Mater 361:129685. https://doi.org/10.1016/j.conbuildmat.2022.129685
3. Xu Q, Solaimanian M (2008) Measurement and evaluation of asphalt concrete thermal expansion and contraction. J Test Eval 36(2):140–149. https://doi.org/10.1520/JTE101024
4. Xu Q, Solaimanian M (2010) Modeling temperature distribution and thermal property of asphalt concrete for laboratory testing applications. Constr Build Mater 24(4):487–497. https://doi.org/10.1016/j.conbuildmat.2009.10.013
5. Wang T, Xiao F, Amirkhanian S, Huang W, Zheng M (2017) A review on low temperature performances of rubberized asphalt materials. Constr Build Mater 145:483–505. https://doi.org/10.1016/j.conbuildmat.2017.04.031
6. Mohajerani A, Bakaric J, Jeffrey-Bailey T (2017) The urban heat island effect, its causes, and mitigation, with reference to the thermal properties of asphalt concrete. J Environ Manage 197:522–538. https://doi.org/10.1016/j.jenvman.2017.03.095
7. Sha A, Liu Z, Tang K, Li P (2017) Solar heating reflective coating layer (SHRCL) to cool the asphalt pavement surface. Constr Build Mater 139:355–364. https://doi.org/10.1016/j.conbuildmat.2017.02.087
8. Shamsaei M, Carter A, Vaillancourt M (2022) A review on the heat transfer in asphalt pavements and urban heat island mitigation methods. Constr Build Mater 359:129350. https://doi.org/10.1016/j.conbuildmat.2022.129350
9. Karlessi, T., Gaitani, N., Synnefa, A., Santamouris, M.: Cool pavements. In: Advances in the Development of Cool Materials for the Built Environment, pp. 104–119 (2013).
10. Qin Y, Zhang X, Tan K, Wang J (2022) A review on the influencing factors of pavement surface temperature. Environ Sci Pollut Res 29(45):67659–67674. https://doi.org/10.1007/s11356-022-22295-3
11. Chen J, Wang H, Li L (2015) Determination of effective thermal conductivity of asphalt concrete with random aggregate microstructure. J Mater Civ Eng 27(12):04015045. https://doi.org/10.1061/(ASCE)MT.1943-5533.0001313
12. Aletba SRO, Hassan NA, Jaya RP, Aminudin E, Mahmud MZH, Mohamed A, Hussein AA (2021) Thermal performance of cooling strategies for asphalt pavement: a state-of-the-art review. J Traffic Transp Eng (Engl Ed) 8(3):356–373. https://doi.org/10.1016/j.jtte.2021.02.001
13. Bobes-Jesus V, Pascual-Muñoz P, Castro-Fresno D, Rodriguez-Hernandez J (2013) Asphalt solar collectors: a literature review. Appl Energy 102:962–970. https://doi.org/10.1016/j.apenergy.2012.08.050
14. Kaphle, R.: Improving the Thermal Properties of Asphalt Concrete to Reduce Urban Heat Island Effects (Doctoral dissertation, The University of Texas at San Antonio) (2018).
15. Abbas, F.A., Alhamdo, M.H.: Thermal performance enhancement of a conductive asphalt solar collector. In AIP Conference Proceedings (Vol. 2775, No. 1). AIP Publishing. https://doi.org/10.1063/5.0140183(2023)
16. Elkholy A, Sadek H, Kempers R (2019) An improved transient plane source technique and methodology for measuring the thermal properties of anisotropic materials. Int J Therm Sci 135:362–374. https://doi.org/10.1016/j.ijthermalsci.2018.09.021
17. Byzyka J, Rahman M, Chamberlain DA (2021) A laboratory investigation on thermal properties of virgin and aged asphalt mixture. Constr Build Mater 305:124757. https://doi.org/10.1016/j.conbuildmat.2021.124757
18. Carlson JD, Bhardwaj R, Phelan PE, Kaloush KE, Golden JS (2010) Determining thermal conductivity of paving materials using cylindrical sample geometry. J Mater Civ Eng 22(2):186–195. https://doi.org/10.1061/(ASCE)0899-1561(2010)22:2(186)
19. Zhao D, Qian X, Gu X, Jajja SA, Yang R (2016) Measurement techniques for thermal conductivity and interfacial thermal conductance of bulk and thin film materials. J Electron Packag 138(4):040802. https://doi.org/10.1115/1.4034605
20. Islam MR, Tarefder RA (2014) Determining thermal properties of asphalt concrete using field data and laboratory testing. Constr Build Mater 67:297–306. https://doi.org/10.1016/j.conbuildmat.2014.03.040
21. Dawson AR, Dehdezi PK, Hall MR, Wang J, Isola R (2012) Enhancing thermal properties of asphalt materials for heat storage and transfer applications. Road Mater Pavement Des 13(4):784–803. https://doi.org/10.1080/14680629.2012.735791
22. Kim D, Lee S, Yang I (2021) Verification of thermal conductivity measurements using guarded hot plate and heat flow meter methods. J Korean Phys Soc 78(12):1196–1202. https://doi.org/10.1007/s40042-021-00177-0
23. Log T, Gustafsson SE (1995) Transient plane source (TPS) technique for measuring thermal transport properties of building materials. Fire Mater 19(1):43–49. https://doi.org/10.1002/fam.810190107
24. Petkova-Slipets R, Zlateva P (2018) Thermal properties of a new pavement material for using in road construction. Civ Environ Eng 14(2):99–104. https://doi.org/10.2478/cee-2018-0013
25. Palacios A, Cong L, Navarro ME, Ding Y, Barreneche C (2019) Thermal conductivity measurement techniques for characterizing thermal energy storage materials–a review. Renew Sustain Energy Rev 108:32–52. https://doi.org/10.1016/j.rser.2019.03.020
26. Martínez-Ibáñez, V., Garrido, M. E., Signes, C. H., & Tomás, R.: Determination of thermal conductivity variation through Modified Transient Plane Source (MTPS), and its relationship with porosity variation on thermally treated Prada limestone. In: IOP Conference Series: Earth and Environmental Science (Vol. 833, No. 1, p. 012026). IOP Publishing (2021). https://doi.org/10.1088/1755-1315/833/1/012026
27. Mamlouk MS, Witczak MW, Kaloush KE, Hasan N (2005) Determination of thermal properties of asphalt mixtures. J Test Eval 33(2):118–126. https://doi.org/10.1520/JTE12592
28. Luca J, Mrawira D (2005) New measurement of thermal properties of superpave asphalt concrete. J Mater Civ Eng 17(1):72–79. https://doi.org/10.1061/(ASCE)0899-1561(2005)17:1(72)

29. Tan S, Low B, Fwa T (1992) Determination of thermal conductivity and diffusivity by transient heating of a thin slab. Build Environ 27(1):71–76. https://doi.org/10.1016/0360-1323(92)90010-M
30. Tan S, Fwa T, Chuai C, Low B (1997) Determination of thermal properties of pavement materials and unbound aggregates by transient heat conduction. J Test Eval 25(1):15–22. https://doi.org/10.1520/JTE11319J
31. Côté J, Grosjean V, Konrad JM (2013) Thermal conductivity of bitumen concrete. Can J Civ Eng 40(2):172–180. https://doi.org/10.1139/cjce-2012-0159
32. Kuvandykova, D., Bateman, R.: A new transient method to measure thermal conductivity of asphalt. Therm. Conduct. 31 (2013)
33. Mirzanamadi R, Johansson P, Grammatikos SA (2018) Thermal properties of asphalt concrete: a numerical and experimental study. Constr Build Mater 158:774–785. https://doi.org/10.1016/j.conbuildmat.2017.10.068
34. Bouguerra A, Aït-Mokhtar A, Amiri O, Diop MB (2001) Measurement of thermal conductivity, thermal diffusivity and heat capacity of highly porous building materials using transient plane source technique. Int Commun Heat Mass Transf 28(8):1065–1078. https://doi.org/10.1016/S0735-1933(01)00310-4
35. Khasawneh MA, Sawalha AA, Aljarrah MT, Alsheyab MA (2023) Effect of aggregate gradation and asphalt mix volumetrics on the thermal properties of asphalt concrete. Case Stud Constr Mater 18:e01725. https://doi.org/10.1016/j.cscm.2022.e01725
36. Mrawira DM, Luca J (2006) Effect of aggregate type, gradation, and compaction level on thermal properties of hot-mix asphalts. Can J Civ Eng 33(11):1410–1417. https://doi.org/10.1139/l06-076
37. Hassn A, Aboufoul M, Wu Y, Dawson A, Garcia A (2016) Effect of air voids content on thermal properties of asphalt mixtures. Constr Build Mater 115:327–335. https://doi.org/10.1016/j.conbuildmat.2016.03.106
38. Hassn A, Chiarelli A, Dawson A, Garcia A (2016) Thermal properties of asphalt pavements under dry and wet conditions. Mater Des 91:432–439. https://doi.org/10.1016/j.matdes.2015.11.116
39. Robertson, E.C.: Thermal properties of rocks: U.S. Geol. Survey, Open-File Report, pp. 88–441 (1988)
40. Clauser C, Huenges E (1995) Thermal conductivity of rocks and minerals. Rock Phys. Phase Relat. Handb. Phys. Constants 3:105–126
41. Tang B, Zhu C, Xu M, Chen T, Hu S (2019) Thermal conductivity of sedimentary rocks in the Sichuan basin, Southwest China. Energy Explor Exploit 37(2):691–720. https://doi.org/10.1177/0144598718804902
42. Yan X, Chen L, You Q, Fu Q (2019) Experimental analysis of thermal conductivity of semi-rigid base asphalt pavement. Road Mater Pavem Des 20(5):1215–1227. https://doi.org/10.1080/14680629.2018.1431147
43. Pan P, Wu S, Hu X, Liu G, Li B (2017) Effect of material composition and environmental condition on thermal characteristics of conductive asphalt concrete. Materials 10(3):218. https://doi.org/10.3390/ma10030218
44. Ren Y, Chen M, Yang T, Wu S, Wang K (2021) Effect of steel slag aggregate on pavement and flame-retardant performance of warm-mixed flame-retardant asphalt concrete. Materials 14(3):635. https://doi.org/10.3390/ma14030635
45. Chen J, Chen X, Dan H, Zhang L (2022) Combined prediction method for thermal conductivity of asphalt concrete based on meso-structure and renormalization technology. Appl Sci 12(2):857. https://doi.org/10.3390/app12020857
46. Cominsky RJ, Huber GA, Kennedy TW, Anderson M (1994) The Superpave Mix Design Manual for New Construction and Overlays (No. SHRP-A-407). Strategic Highway Research Program, Washington, DC
47. Mehling, H., Cabeza, L.F.: Heat and cold storage with PCM. Heat and mass transfer, 11–55 (2008)
48. Tritt, T.M. (Ed.).: Thermal conductivity: theory, properties, and applications (2005).
49. Bahia, H.U., Coenen, A., Tabatabaee, N.: Mixture design and compaction. In: Advances in Interlaboratory Testing and Evaluation of Bituminous Materials: State-of-the-Art Report of the RILEM Technical Committee 206-ATB, pp. 85–142 (2013).
50. Demirtürk D, Ozturk HI, Guler M (2024) Investigation of the influence of mixture and microstructural properties on the thermal conductivity of asphalt concrete using the transient heat transfer method. Mater Struct 57(8):179. https://doi.org/10.1617/s11527-024-02456-1

Publisher's Note Springer Nature remains neutral with regard to jurisdictional claims in published maps and institutional affiliations.